Journal of
Synchrotron
Radiation

ISSN 0909-0495

Received 25 November 2004
Accepted 14 April 2005

Protein nanocrystallography: growth mechanism and atomic structure of crystals induced by nanotemplates

E. Pechkova,[a,b] F. Vasile,[b] R. Spera,[b] S. Fiordoro[a] and C. Nicolini[a,b]*

[a]Fondazione ElBA, Via delle Testuggini, Roma, Italy, and [b]Nanoworld Institute and Biophysics Division, University of Genoa, Corso Europa 30, 16132 Genoa, Italy.
E-mail: manuscript@ibf.unige.it

Protein nanocrystallography, a new technology for crystal growth based on protein nanotemplates, has recently been shown to produce diffracting, stable and radiation-resistant lysozyme crystals. This article, by computing these lysozyme crystals' atomic structures, obtained by the diffraction patterns of microfocused synchrotron radiation, provides a possible mechanism for this increased stability, namely a significant decrease in water content accompanied by a minor but significant α-helix increase. These data are shown to be compatible with the circular dichroism and two-dimensional Fourier transform spectra of high-resolution H NMR of proteins dissolved from the same nanotemplate-based crystal *versus* those from a classical crystal. Finally, evidence for protein direct transfer from the nanotemplate to the drop and the participation of the template proteins in crystal nucleation and growth is provided by high-resolution NMR spectrometry and mass spectrometry. Furthermore, the lysozyme nanotemplate appears stable up to 523 K, as confirmed by a thermal denaturation study using spectropolarimetry. The overall data suggest that heat-proof lysozyme presence in the crystal provides a possible explanation of the crystal's resistance to synchrotron radiation.

Keywords: protein crystals; mass spectroscopy; NMR; CD.

1. Introduction

The term 'protein nanocrystallography' (Pechkova & Nicolini, 2003, 2004*a*; Nicolini & Pechkova, 2004) has been accepted by both crystallographic (*e.g.* Pechkova *et al.*, 2003) and nanotechnological (*e.g.* Pechkova & Nicolini, 2002*b*) communities.

Protein nanocrystallography has been defined as being at the intersection between nanotechnology and proteomics. This emerging field results from the combination of advanced nanotechnologies, particularly atomic force microscopy , thin-film nanotemplate technology, nanogravimetry and microfocused synchrotron radiation. It should be noted that nanocrystallography does not refer to the study of self-assembled organic and inorganic crystals of nanometer size or nanoparticles. In addition, it does not refer to the nanodrop or microdrop crystallization technology resulting from the exciting advances made in microfluid chips (Thorsen *et al.*, 2002).

Furthermore, the term does not refer to so-called protein nanocrystals; the protein nanocrystalline state or powder consists of aggregates smaller than 1 μm in size, usually occurring in the amorphous precipitate, the method of preparation and characterization of this nanocrystalline matter being the same as that of the large crystals obtained with increased concentration of the protein and/or the precipitant (Martin & Zilm, 2003). A more appropriate terminology would be 'protein nanoaggregates', even if in some cases these substances have been proved to be ordered. In order to see real crystal order, one needs to consider the micrometre size.

In summary, we can properly refer to nanocrystallography only when the method of crystallization and characterization is based on nanotechnology. Protein nanocrystallography has indeed been successful in crystallization of proteins that had not previously been crystallized, such as membrane protein cytochrome P450scc (Pechkova & Nicolini, 2002*a*,*b*; Nicolini & Pechkova, 2004), and in solving the structures of proteins that were previously unknown, for example CK2 human kinase (Pechkova & Nicolini, 2004*b*), pointing to a very promising nanotechnology-based approach in structural proteomics.

Lysozyme is a hydrolase enzyme (EC 3.2.1.17) which, thanks to exceptional ease of crystallization, is frequently used as an example in protein crystallization studies, such as

investigations into the effects of impurities, pH and temperature on crystallization mechanisms (Yoshizaki *et al.*, 2004); studies of nucleation rates (Forsythe *et al.*, 2002; see Garcia-Ruiz, 2003 for review); microscopic (atomic level) mathematical modelling including statistical mechanics and lattice simulations of nucleation (see Kierzek & Zielenkiewicz, 2001 for review); macroscopic mathematical modelling of crystallization kinetics (Manno *et al.*, 2003; Agena *et al.*, 1999; Bessho *et al.*, 1994); and X-ray topography and diffraction analysis of crystal perfection, growth, quality, response to humidity and dislocations (Tachibana *et al.*, 2003; Hu *et al.*, 2001; Dobrianov *et al.*, 2001, 1998; Boggon *et al.*, 2000).

Lysozyme is also routinely used as a test object when a new technique needs to be verified (Adachi *et al.*, 2004; Kadowaki *et al.*, 2004; van der Woerd *et al.*, 2003; Sanjoh *et al.*, 2001; Penkova *et al.*, 2002; Tsekova *et al.*, 1999; Chayen *et al.*, 2001). In our work, lysozyme was initially used as a model protein in the investigation of the influence of Langmuir–Blodgett (LB) nanofilms on crystallization, crystal quality, and eventual structure of the protein and its aqueous environment in the crystal. We initially found that LB coating on the cover slide of common crystallization plates leads to stimulation of protein crystal growth, allowing the acceleration of the lysozyme crystal growth rate compared with the classical vapour diffusion method (Pechkova & Nicolini, 2001). Radiation-stable microcrystals with pronounced diffraction patterns were then reproducibly obtained by the nanotechnology-based method (Pechkova & Nicolini, 2003, and references therein) for proteins cytochrome P450scc and human kinase CK2, for which attempts at crystallization using conventional methods were unsuccessful. It is important to note that the use of microcrystals for X-ray diffraction studies requires microfocused synchrotron radiation, and therefore a higher flux density than that used for routine protein crystallography with synchrotron radiation was applied to the crystals.

However, atomic resolution structure has been derived at the ESRF microfocus beamline from minuscule protein microcrystals with diameters of 20 µm, for which attempts at crystallization using conventional methods were unsuccessful (Pechkova & Nicolini, 2004*b*; Pechkova *et al.*, 2003). The solution of the crystal structure required a high flux density of microfocused synchrotron radiation. In the course of data collection on these proteins and on lysozyme crystals obtained by the nanotemplate method, it appeared that the crystals showed a particularly long lifetime in the beam, which suggested less sensitivity to radiation damage (Pechkova *et al.*, 2004). The aim of the present report is to obtain data of a more quantitative nature on this phenomenon and to propose a model.

The exact mechanism by which the presence of LB nanofilms accelerates and guides crystallization is not clear, even though it is quite evident that the primary physical factor is the anisotropy rendered by the film to the growing crystal. This anisotropy possibly has an electrostatic nature, since dipole moments of protein monomers are oriented identically in the film, as confirmed by surface potential measurements (Pechkova & Nicolini, 2003, and references therein).

The present study attempts to determine whether introduction of an LB nanofilm modifies the three-dimensional structure of the protein and/or the configuration of water molecules surrounding the protein. We determined the three-dimensional atomic structure of lysozyme in the nanofilm-based and the classical crystals with synchrotron radiation using the molecular replacement method and by ^{1}H NMR spectrometry. Apart from the above considerations, we chose lysozyme because any improvement of the crystal quality upon LB film introduction, considering that the quality of the classical lysozyme crystals is already high, could imply that the method has enormous potential for proteins that are not so readily crystallizable.

Furthermore, in order to understand the role of the nanotemplate in lysozyme crystallization, we used flourescein labelling of the proteins forming the LB film used as the nanotemplate. Fluorescein labelling of proteins is usually performed through either the side-chain amino group of a lysine residue or the side-chain sulfhydryl group of a cysteine residue, using commercially available linkers. The side-chain amino group labels include fluorescein–succinimidyl derivatives for specific labelling of NH_2 sites (Vives & Bernard, 2003). We used carboxyfluorescein succinimidyl ester (CFSE) rather than fluorescein isothiocyanate, resulting in more reliable labelling. The crystals obtained in the presence of CFSE-labelled templates were analysed by ^{1}H NMR spectrometry and mass spectrometry in order to establish if template proteins directly transfer from the nanofilm to the drop solution and participate in crystal formation.

2. Methods

Chicken egg-white lysozyme was purchased from Sigma.

2.1. Fluorescein labelling of lysozyme

A solution of CFSE with a concentration of 1.5 mg ml^{-1} was prepared in anhydrous dimethylsulfoxide. A CFSE solution (100 µl) was added to a protein lysozyme solution (1 ml) with a concentration of 1 mg ml^{-1}. The mixture was incubated for 90 min in the dark at room temperature with continuous gentle agitation. Labelled protein was separated from free fluorescein compounds by extensive dialysis *versus* phosphate-buffered saline (overnight). The protein was concentrated with Centricon concentrators up to 40 mg ml^{-1}, centrifuged for 10 min at high speed and filtered through a 0.22 µm filter.

2.2. Lysozyme nanotemplate formation and crystallization

Lysozyme or CFSE-labelled lysozyme (about 600 µl with concentration 40 mg ml^{-1}) was spread on the air–water interface of an LB trough and compressed by surface pressure (20 mN m^{-1}). The protein monolayer was transferred by the Langmuir–Schaeffer method onto the siliconized glass cover slide used for crystallization. Lysozyme crystallization by the classical method and by nanotemplating are described in detail by Pechkova & Nicolini (2001).

2.3. Synchrotron radiation

Diffraction data were collected at a temperature of 100 K. Crystals were removed from the mother liquor and frozen in a nitrogen stream using cryoprotectant from Hampton Research. One nanotemplate and one classical crystal of the same dimensions (see Fig. 1) were used to collect the complete data sets at the microfocus beamline ID-13 at the ESRF (Riekel, 2004). The beam size was 5 µm × 5 µm; the wavelength used was 0.9755 Å and the crystal-to-detector distance was 100 mm. Crystals diffracted to a maximum resolution of 1.7 Å.

The lysozyme crystals belong to space group $P4_32_12$, with unit-cell parameters (classical/LB-based) $a = b = 78.89/79.21$ Å and $c = 37.16/37.42$ Å. One molecule is present in the asymmetric unit. Assuming a molecular mass of approximately 14000 Da, the V_M coefficient is about 2.09 Å. Standard procedures of data reduction were followed using the *MOSFLM* and *SCALA* programs from the *CCP*4 suite (Wild *et al.*, 1995). The phase problem was solved using the molecular replacement method using the software package *CNS* (Brünger *et al.*, 1998), and the three-dimensional structure was determined from a map using the software package *QUANTA* (http://www.accelrys.com/quanta/quanta.html), *via* map skeletonization and secondary-structure determination, and the package *XtalView* (McRee, 1992), *via* direct fitting of Cα atoms. Refinement was performed manually using both packages, and finally by the *CCP*4 program *REFMAC*5.

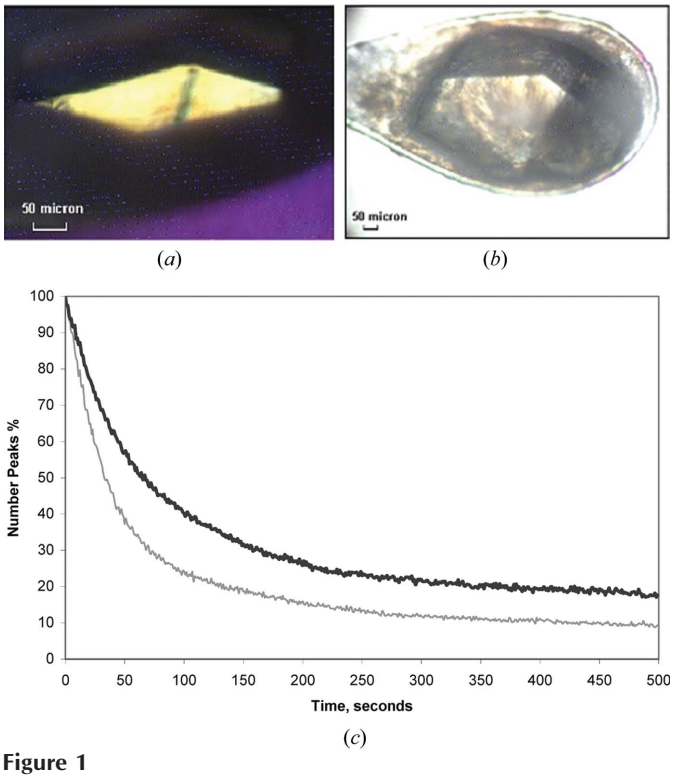

Figure 1
Lysozyme crystal prepared (*a*) by the classical hanging-drop method and (*b*) by the nanobiofilm template method after 500 s of intense focused radiation exposure. (*c*) Number of reflections *versus* time of radiation exposure for lysozyme crystals grown with (black line) and without (grey line) a nanobiofilm template.

2.4. Nuclear magnetic resonance spectroscopy

^{1}H NMR experiments were recorded on a Bruker AMX 500 MHz device on a Silicon Graphics SGI O2 (OS IRIX 6.3).

The probe temperature was maintained at 300 K, and water suppression was carried out using a watergate and the DPFGSE scheme. The spectral width was about 16 p.p.m. (Pulsinelli *et al.*, 2003).

The sample for NMR measurements was obtained by dissolving a sufficient number of crystals in water (0.5 ml, with 10% D_2O) to obtain a 0.6–0.8 m*M* concentration. The NMR spectra were analysed using the *XEASY* program (Bartels *et al.*, 1995). As reference for protein assignment we take into account the work of Redfield and co-workers (Redfield *et al.*, 1998).

2.5. Mass spectrometry methods

The mass spectrometry measurements were performed on a Bruker Autoflex matrix-assisted laser desorption/ionization time-of-flight (MALDI-TOF) mass spectrometer (Bruker Daltonics, Leipzig, Germany) to monitor the purity of the protein solutions before and after being crystallized and to verify the presence of CFSE-labelled molecules in the crystal.

The control sample of a 2 n*M* solution of lysozyme was prepared by dissolving protein lyophilized powder (Sigma–Aldrich) in 0.1% trifluoroacetic acid (TFA). Lysozyme crystals obtained by nanotemplate and CFSE-labelled nanotemplate methods were dissolved in 0.1% TFA for analysis.

For protein fingerprinting, the lysozyme samples were digested with trypsin; the sample was dissolved/diluted in 100 m*M* ammonium bicarbonate (Sigma–Aldrich) pH 8.5, and trypsin dissolved in 1 m*M* HCl to a concentration of 1 mg ml^{-1} was added. The solutions were incubated for 3 h at 310 K.

The matrix used for the mass spectrometry analysis was a saturated solution of α-cyano-4-hydroxycinnamic acid (Bruker Daltonics) dissolved in a mixture of two-thirds 0.1% TFA and one-third acetonitrile. Analytes were spotted onto an aluminium plate. We used the 'dried droplet method' for the sample deposition; before deposition, the matrix was mixed in with the sample, and then 1 µl of this mixture was deposited on the plate. The final concentration utilized for each sample was 1 n*M*.

The obtained mass lists were compared with database lists for the protein identification (Bonk & Humeny, 2001). For protein data interpretation we used the *Biotools* software (Bruker Daltonics), which allows automated protein identification *via* a library search and has *MASCOT* intranet search software (Matrix Sciences) fully integrated. We analysed three lysozyme samples (lyophilized powder dissolved in 0.1% TFA, marked lysozyme and pure lysozyme crystals dissolved in 0.1% TFA). For the intact protein analysis we used a MALDI mass spectrometer in linear mode, with a scanning range from 4 to 20 kDa, obtaining a resolution of about 500; for the analysis of the peptides obtained from the tryptic digestion of the samples, we used the mass spectrometer in reflectron

Table 1
Parameter comparison of reflection data, electron density maps and three-dimensional structures between the classical and the LB crystals of lysozyme.

	Classical	LB-based
Beamline	Microfocus ID13, ESRF	Microfocus ID13, ESRF
Temperature (K)	100	100
Detector	MAR CCD	MAR CCD
Wavelength (Å)	0.9755	0.9755
Space group	$P4_32_12$	$P4_32_12$
Unit-cell parameters (Å, °)	a = 78.89	a = 79.21
	b = 78.89	b = 79.21
	c = 37.16,	c = 37.42
	$\alpha = \beta = \gamma = 90$	$\alpha = \beta = \gamma = 90$
Resolution range	27–1.7	27–1.7
Independent reflections	13046	13598
Map fragmentation (%)	12	5
Total correlation coefficient between map and three-dimensional structure†	0.758	0.726
α-Helix content, residues	42	45
Quantity of water molecules resolved per lysozyme molecule at 100σ threshold	63	53
Quantity of water molecules modelled in a 60 Å-diameter sphere (including those resolved)	4933	4669

† Water is not included because of different quantities of water molecules resolved.

mode, with a scanning range between 500 and 2000 Da, obtaining a resolution between 2000 and 6000. To calibrate the mass spectrometer we used protein and peptide calibration standard solutions (Bruker Daltonics).

2.6. Circular dichroism (CD)

CD spectra were recorded on a Jasco J-700 spectropolarimeter at physiological ionic strength. All spectra were recorded in a nitrogen atmosphere at room temperature using a 0.05 cm path-length quartz cell. Each spectrum is an average of ten scans over 300–190 nm.

3. Results

The crystals formed by nanotemplating are dramatically different from classical crystals in terms of stability to synchrotron radiation, as proven in Fig. 1. In the classical crystal, the number of reflections in the diffraction pattern decay quite fast and damage appears only 500 s after exposure (for details see Pechkova *et al.*, 2004).

To facilitate comparison of the differences in the structures derived from classical and LB-based crystals, we assessed the overall characteristics of the crystals by comparing the initial reflection data, the maps derived from them and the three-dimensional structures obtained. These results are summarized in Table 1.

Generally, the differences between the structures of the lysozyme molecules themselves are very small: only about 0.28 Å r.m.s. difference between the LB-based and the classical structures when they are superimposed. After refinement, this difference reduces to 0.17 Å. However, the lysozyme molecules appear oriented differently with respect to the crystal axes; this difference might be related to differences in hydrogen bonding with water molecules.

Table 2
Secondary structure of water-dissolved lysozyme crystals derived from the modified vapour diffusion method with (nanotemplate crystal) and without (classical crystals) lysozyme thin film used as the nanotemplate.

The percentages of the various types of secondary structure are indicated. For reference, the percentage of α-helix in lysozyme thin film is 40%.

	α-Helix	β-Sheet	β-Turn	Random coil
Nanotemplate crystals	36.6	25.2	7.4	30.8
Classical crystals	28.4	28.6	10.5	32.5

This supposition prompted us to analyse the arrangement of water molecules around the lysozyme molecule; this arrangement indeed exhibits a much larger difference. A smaller number of water molecules were resolved for the LB crystal at high threshold than for the classical crystal. We have chosen such a high threshold to be certain that all of the resolved water molecules immediately adhere to the protein surface. To estimate how water will surround the lysozyme molecule in a crystal, water molecules were modelled by expanding the already resolved water layer, to fill a 60 Å-diameter sphere, for both the classical and the LB crystals. Such a modelling technique repeats the surface topology of the protein and the adherent water layer, and is therefore suitable for modelling water in a crystal. At this point, the difference in water content is estimated to be about 6% smaller for LB crystals (4669 *versus* 4933 molecules), which is augmented by the fact that the unit-cell volume is somewhat larger (235 *versus* 231 nm^3) for the LB crystals. For proteins, a higher level of hydrogen bonding invariably leads to increased secondary-structure content, particularly with respect to α-helices that are largely held together by hydrogen bonds. Indeed, slightly increased α-helicity is observed for the LB crystal (Table 1).

CD spectra taken between 180 and 250 nm confirm the minor increase of α-helix in a crystal grown by nanotemplate with respect to the classical crystal (Table 2).

In order to have an additional independent confirmation of this very critical structural difference we have also analysed, by 500 MHz H NMR, the conformation of lysozyme crystals obtained from LB film (Fig. 2). Our goal is to verify if there are some conformational differences between our crystals and the lysozyme protein that has not experienced LB packing. The monodimensional NMR spectra of a protein crystal grown on LB film and of a lysozyme sample from a classical crystal (not shown) suggest that the general folds of the molecules are maintained and only minor differences are evidenced. To characterize the structure obtained by LB crystals, and to investigate the difference in helical content as evidenced by CD spectra (Table 2), we performed (Fig. 2) TOCSY and NOESY (total correlation and nuclear Overhauser effect spectroscopy). If we compare our TOCSY spectrum with the data published by Poznanski *et al.* (2003), we can observe the

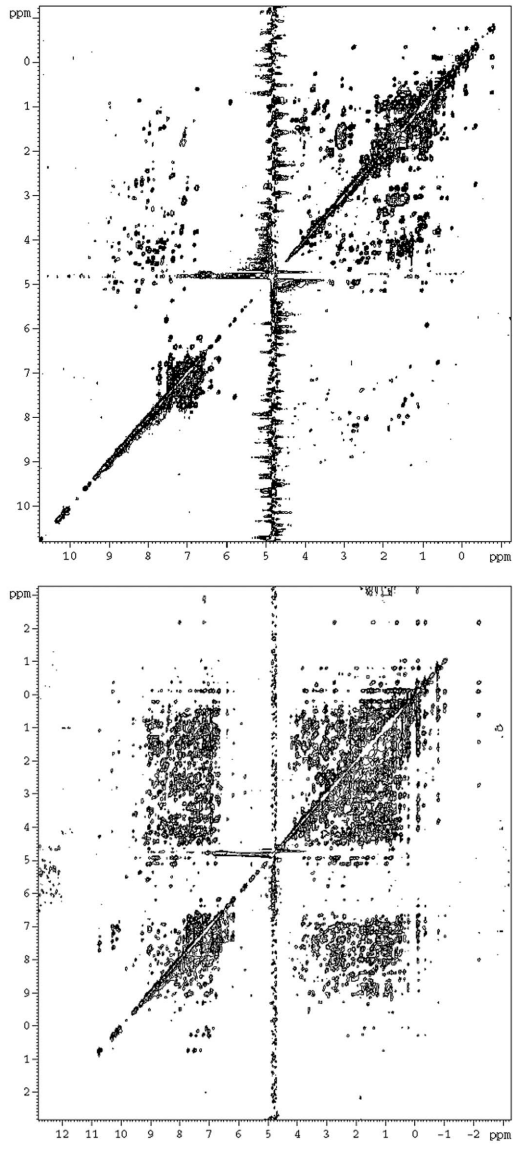

Figure 2
500 MHz TOCSY and NOESY (mixing time = 300 ms) spectra of a lysozyme crystal grown on LB film.

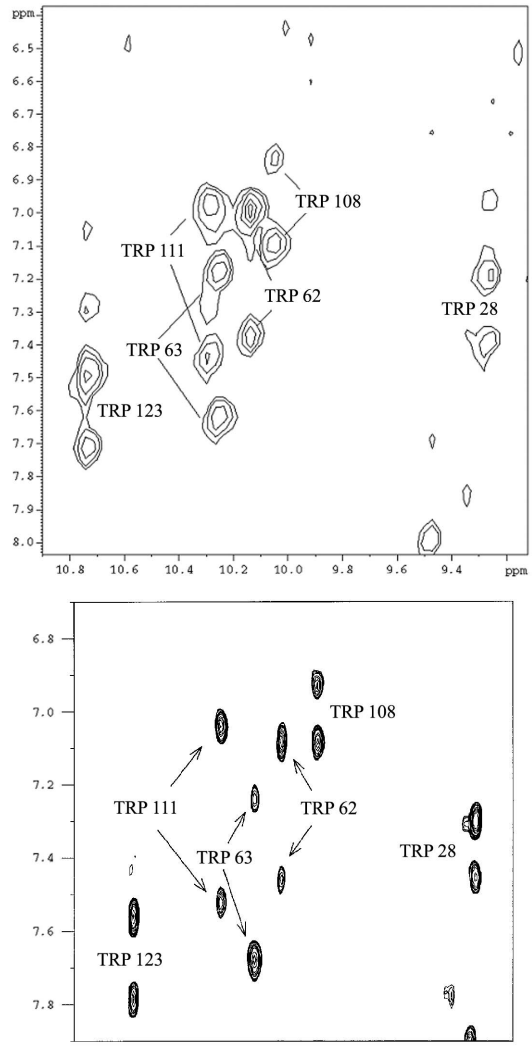

Figure 3
500 MHz NOESY spectrum (mixing time = 300 ms) of a lysozyme crystal grown on film: He1/Hd1 and He1/Hz2 correlation of tryptophans (above). If we compare this region with the same range observed by Kristiansen *et al.* (1998) (below), we can observe some differences in the resonance positions of tryptophans aromatic H atoms, indicating small conformational differences between the two analysed proteins.

presence of significant differences in the fingerprint regions of the two spectra.

By comparison with the above fingerprint of a standard NMR spectrum of lysozyme, the differences in the resonances of NH/HA suggest a different lysozyme conformation.

In order to discover if our protein from LB crystals differs from lysozyme from classical crystals, we analysed the region of the tryptophan side chains in the NOESY spectrum (Fig. 3), and we observed some difference in the resonance position of tryptophan aromatic H atoms, indicating that significant small conformational differences exist between the two analysed proteins.

From the MALDI mass spectrometer analysis of the intact protein spectra, we also verified that after crystallization and the successive dissolution the protein was still pure (Fig. 4*a*), corroborating all of the above NMR studies.

Subsequently, we explored the mechanism of crystal nucleation and growth in the presence of nanotemplates, by selectively labelling the LB protein film serving as template in the vapour diffusion and by monitoring its eventual presence in the crystal being formed. Evidence for protein direct transfer from the nanotemplate to the drop and the participation of template protein in crystal nucleation and growth is indeed provided by high-resolution NMR spectrometry (Fig. 5) and mass spectrometry (Fig. 4*b*).

It is possible to note that the CFSE molecule appears bound to the lysozyme crystal being formed by nanotemplate-based vapour diffusion, where the CFSE molecule has, in fact, the expected mass of 473 Da.

Similarly, if we analyse by ^{1}H NMR the complex obtained between lysozyme and (6)-carboxyfluorescein-*N*-hydroxysuccinimide ester (Fig. 5) we observe that the general fold of

the lysozyme is conserved. In fact, the NH regions of the one-dimensional NMR spectra (even if the spectrum obtained for the complex, particularly in this region, shows a poor signal-to-noise ratio as a result of the low concentration of the sample) show a similar spread of peaks and no significant change in proton chemical shifts can be observed. On the other hand, in this region new peaks appear as a result of the fluorescent ligand and some peaks of the protein are less sharp (compared with the spectrum of the protein alone) probably due to the interaction with CFSE.

In the aliphatic region of the spectra, between −2.0 and 4.5 p.p.m., significant differences occur at the level of the peak at 1.3 p.p.m. and in the multiplicity of the signal at 0.7 p.p.m., indicating that the protein experiences some conformational changes, as a result of binding with fluorescein. Interestingly, the thermal stability of lysozyme in the nanotemplate appears higher (up to 523 K) than that for the same protein in solution (about 348 K), as shown by the dependence of molar ellipticity at 195 nm on temperature in the range 298–523 K (Fig. 6).

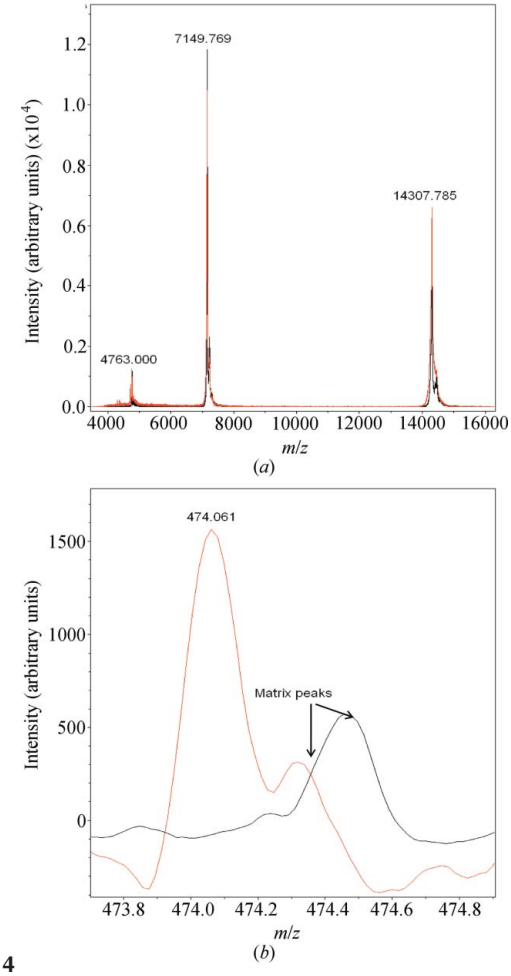

Figure 4
(Top) In black, the spectrum of pure lysozyme from lyophilized powder dissolved in 0.1% TFA, and in red, the spectrum of a marked lysozyme crystal. The three peaks were assigned as $[m]^+$ for m/z = 14307.785, $[m]^{2+}$ (double charge) for m/z = 7149.769 and $[m]^{3+}$ (triple charge) for m/z = 4763.4763. There is no evidence of peak shifts. (Bottom) Low weights detail: in black, the spectrum of pure lysozyme, and in red, the spectrum of a marked lysozyme crystal. The peak at 474 Da (CFSE) is evidently present only in the red spectrum.

4. Discussion

All of the above data obtained by X-ray synchrotron diffraction, NMR, circular dichroism and thermal denaturation point, for the nanotemplate-produced lysozyme crystal, to a minor but consistent increase in the fraction of α-helix, which appears compatible with the observed decrease in water content, the increased thermal stability and the increased resistance to synchrotron radiation.

The LB crystal appears to be superior to the classical crystal with respect to map fragmentation and map correlation to the resulting models. The higher quality of the LB crystal with respect to the classical crystal can again be ascribed to higher water ordering brought about by the presence of the film. It

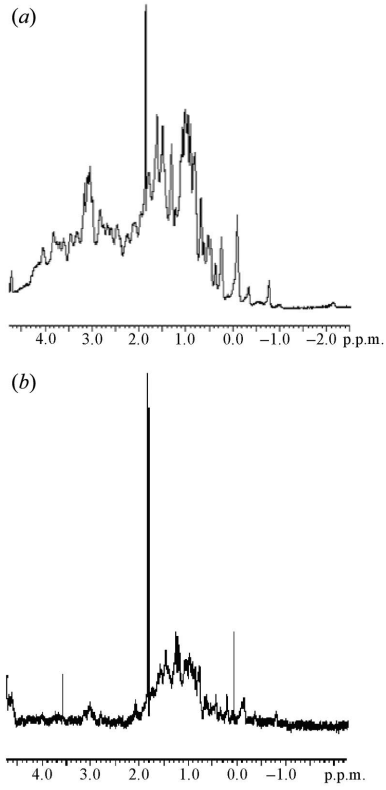

Figure 5
NMR spectra of a lysozyme crystal (*a*) and of a lysozyme/fluorescein complex (*b*). The region between −2.0 and 4.5 p.p.m. is shown.

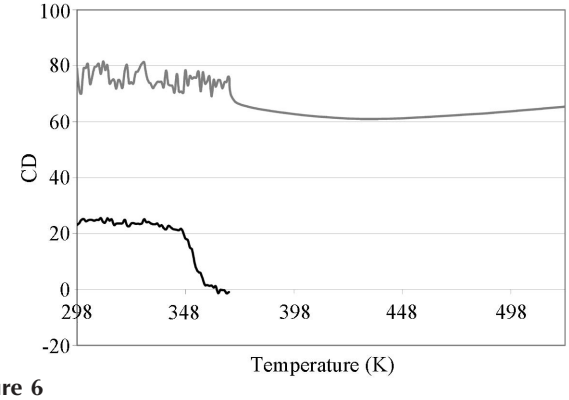

Figure 6
Molar ellipticity at 196 nm *versus* temperature for lysozyme LB film (upper grey line) as compared with lysozyme solution (lower black line).

should be noted that the estimated protein dehydration in the crystal parallels that reported for protein in an LB film (Nicolini, 1997).

Comfortingly, in the present communication, which aimed also to investigate the lysozyme crystal growth mechanisms with and without nanotemplating, lysozyme appears to transfer directly from the nanostructured film to the drop to trigger the formation of the crystal, therefore highlighting the physical interpretation of the mechanism for nanotemplate-induced protein crystallization.

This project was supported by an FIRB grant to the Fondazione ElBA and to the Nanoworld Institute of the University of Genova by the MIUR on Organic Nanosciences and Nanotechnologies, by an FISR on Nanotechnology by the MIUR to Fondazione ElBA, and by a grant on Nanotechnology to the Fondazione ElBA by CNR of Italy. The authors are grateful to Mrs Cristina Rando and Mr Fabrizio Nozza for technical support.

References

Adachi, H., Takano, K., Matsumura, H., Inoue, T., Mori, Y. & Sasaki, T. (2004). *J Synchrotron Rad.* **11**, 121–124.
Agena, S. M., Pusey, M. L. & Bogle, I. D. (1999). *Biotechnol. Bioeng.* **64**, 144–150.
Bartels, Ch., Xia, T.-H., Billeter, M., Güntert, P. & Wüthrich, K. (1995). *J. Biomol. NMR*, **5**, 1–10.
Bessho, Y., Ataka, M., Asai, M. & Katsura, T. (1994). *Biophys. J.* **66**, 310–313.
Boggon, T. J., Helliwell, J. R., Judge, R. A., Olczak, A., Siddons, D. P., Snell, E. H. & Stojanoff, V. (2000). *Acta Cryst.* D**56**, 868–880.
Bonk, T. & Humeny, A. (2001). *Neuroscientist*, **7**, 6–12.
Brünger, A. T., Adams, P. D., Clore, G. M., DeLano, W. L., Gros, P., Grosse-Kunstleve, R. W., Jiang, J.-S., Kuszewski, J., Nilges, M., Pannu, N. S., Read, R. J., Rice, L. M., Simonson, T. & Warren, G. L. (1998). *Acta Cryst.* D**54**, 905–921.
Chayen, N. E., Saridakis, E., El-Bahar, R. & Nemirovsky, Y. (2001). *J. Mol. Biol.* **312**, 591–595.
Dobrianov, I., Finkelstein, K. D., Lemay, S. G. & Thorne, R. E. (1998). *Acta Cryst.* D**54**, 922–937.
Dobrianov, I., Kriminski, S., Caylor, C. L., Lemay, S. G., Kimmer, C., Kisselev, A., Finkelstein, K. D. & Thorne, R. E. (2001). *Acta Cryst.* D**57**, 61–68.
Forsythe, E. L., Maxwell, D. L. & Pusey, M. (2002). *Acta Cryst.* D**58**, 1601–1605.
Garcia-Ruiz, J. M. J. (2003). *Struct. Biol.* **142**, 22–31.
Hu, Z. W., Thomas, B. R. & Chernov, A. A. (2001). *Acta Cryst.* D**57**, 840–846.
Kadowaki, A., Yoshizaki, I., Rong, L., Komatsu, H., Odawara, O. & Yoda, S. (2004). *J Synchrotron Rad.* **11**, 38–40.
Kierzek, A. M. & Zielenkiewicz, P. (2001). *Biophys. Chem.* **91**, 1–20.
Kristiansen, A., Varum, K. M. & Grasdalen, H. (1998). *Eur. J. Biochem.* **251**, 335–342.
McRee, D. E. (1992). *J. Mol. Graph.* **10**, 44–46.
Manno, M., Xiao, C., Bulone, D., Martorana, V. & San Biagio, P. L. (2003). *Phys. Rev. E*, **68**, 119–204.
Martin, R. W. & Zilm, K. W. (2003). *J. Magn. Reson.* **165**, 162–174.
Nicolini, C. (1997). *Trends Biotechnol.* **15**, 395–401.
Nicolini, C. & Pechkova, E. (2004). *Expert Rev. Proteom.* **1**, 253–256.
Pechkova, E. & Nicolini, C. (2001). *J. Cryst. Growth*, **231**, 599–602.
Pechkova, E. & Nicolini, C. (2002*a*). *J. Cell. Biochem.* **85**, 243–251.
Pechkova, E. & Nicolini, C. (2002*b*). *Nanotechnology*, **13**, 460–464.
Pechkova, E. & Nicolini, C. (2003). *Proteomics and Nanocrystallography*. New York: Kluwer Academic/Plenum.
Pechkova, E. & Nicolini C. (2004*a*). *Trends Biotechnol.* **22**, 117–122.
Pechkova, E. & Nicolini, C. (2004*b*). *J. Cell. Biochem.* **91**, 1010–1020.
Pechkova, E., Tropiano, G., Riekel, C. & Nicolini, C. (2004). *Spectrochim. Acta B*, **59**, 1687–1693.
Pechkova, E., Zanotti, G. & Nicolini, C. (2003). *Acta Cryst.* D**59**, 2133–2139.
Penkova, A., Chayen, N., Saridakis, E. & Nanev, C. N. (2002). *Acta Cryst.* D**58**, 1606–1610.
Poznanski, J., Georgalis, Y., Wehr, L., Saenger, W. & Zielenkiewicz, P. (2003). *Biophys. Chem.* **104**, 605–616.
Pulsinelli, E., Vasile, F., Vergani, L., Parodi, S. & Nicolini, C. (2003). *Protein Pept. Lett.* **10**, 541–549.
Redfield, C. & Dobson, C. M. (1998). *Biochemistry*, **27**, 122–136.
Riekel, C. (2004). *J. Synchrotron Rad.* **11**, 4–6.
Sanjoh, A., Tsukihara, T. & Gorti, S. (2001). *J. Cryst. Growth*, **232**, 618–628.
Tachibana, M., Koizumi, H., Izumi, K., Kajiwara, K. & Kojima, K. (2003). *J. Synchrotron Rad.* **10**, 416–420.
Thorsen, T., Maerkl, S. J. & Quake, S. R. (2002). *Science*, **298**, 580–584.
Tsekova, D., Dimitrova, S. & Nanev, C. N. (1999). *J. Cryst. Growth*, **196**, 226–233.
Vives, E. & Bernard, L. (2003). *Tetrahedron Lett.* **44**, 5389–5391.
Wild, D. L., Tucker, P. A. & Choe, S. (1995). *J. Mol. Graph.* **13**, 291–298.
Woerd, M. van der, Ferree, D. & Pusey, M. (2003). *J. Struct. Biol.* **142**, 180–187.
Yoshizaki, I., Kadowaki, A., Iimura, Y., Igarashi, N., Yoda, S. & Komatsu, H. (2004). *J. Synchrotron Rad.* **11**, 30–33.